Pak. J. Chem. 16(1-2): 19-29, 2026 Research article
ISSN (Print): 2220-2625
ISSN (Online): 2222-307X DOI: 10.15228/2026.v16.i1-2.p03

# Multifunctional Chitosan-Based Synergized Nanocomposite Films with Enhanced Mechanical Strength, Electrical Conductivity, and Antioxidant Activity

Srosh Fazil[1], Khurram Liaqat*[1], Danish Anwar[1], Imtiaz Hussain[2], Syed Fakhar Alam[3]
[1] Department of Chemistry, University of Poonch Rawalakot, Rawalakot 12350, Azad Kashmir, Pakistan.
[2] Department of Food Science and Technology, University of Poonch Rawalakot, Rawalakot 12350, Azad Kashmir, Pakistan.
[3]LEJ Nanotechnology Center, H.E.J. Research Institute of Chemistry, International Center for Chemical and Biological Sciences (ICCBS), University of Karachi, Karachi (75270), Pakistan.
**Corresponding Author email**: khurramliaqat@upr.edu.pk

## Abstract
This study presents a systematic approach for the synthesis of synergized nanocomposite films (SNCFs) by incorporating graphene oxide (GO) and varying weight ratios of multiwalled carbon nanotubes (MWCNTs) into a chitosan (Ch) matrix via a solution-blending method. The resulting films were comprehensively characterized to evaluate their structural, thermal, mechanical, electrical, and antioxidant properties. Fourier-transform infrared spectroscopy (FTIR) revealed distinct peak shifts, while X-ray diffraction (XRD) showed peak suppression and broadening, providing direct evidence of strong interfacial interactions, including hydrogen bonding and π–π stacking, which facilitate efficient interfacial charge transfer between chitosan, GO, and MWCNTs. SEM and XRD analyses further confirmed the successful synthesis of a uniformly dispersed nanocomposite comprising nanoscale GO sheets and entangled MWCNT networks embedded within the chitosan matrix. Thermogravimetric analysis demonstrated enhanced thermal stability of the SNCFs compared to pristine chitosan. Significant improvements in tensile strength and modulus were observed with increasing MWCNT content, accompanied by a reduction in elongation at break. Electrical conductivity exhibited a pronounced enhancement, with a percolation threshold identified in the range of 0.03–0.05 wt.% MWCNTs. Moreover, antioxidant activity increased markedly, reaching approximately 90% enhancement at 0.09 wt.% MWCNTs combined with 0.05 wt.% GO. These multifunctional enhancements are attributed to synergistic electron-transfer processes and strong interfacial interactions within the hybrid nanofiller network.

**Keywords**: Nanocomposite Films (NCFs), Synergized nanocomposite films (SNCFs), Multiwalled Carbon nanotubes (MWCNTs), Graphene Oxide (GO), Tensile strength and Antioxidant Activity

## 1. Introduction
The integration of electrically conductive polymers into food and biological processes poses several significant challenges, mainly due to cytotoxicity, low biodegradability, and poor biocompatibility. An effective plan to overcome these issues would be to incorporate electrically conductive fillers into naturally available biocompatible polymers [1-5]. Chitosan (Ch), one of the most researched biopolymers due to its characteristics such as abundance, renewability, biodegradability, and non-toxicity, has found many applications in food packaging and medicine for its natural antibacterial and antioxidant properties [6–10]. However, the mechanical and electrical properties of chitosan are too low and, accordingly, it requires the addition of suitable fillers to increase its functionality [11, 12]. Among the possible fillers, carbon nanofillers, in particular carbon nanotubes (CNTs) and graphene oxide (GO), are the most promising, as they possess high mechanical, thermal, and electrical properties and a large specific surface area [13, 14]. The polymer/carbon composites are prepared by carefully combining polymers with carbon nanofillers. The effectiveness of these composites depends strongly on the homogenization of nanosized fillers, which in turn depends on aggregation and quantum-size effects [15]. Carbon nanotubes (CNTs) are valued for their exceptional mechanical properties and high aspect ratios. Nonetheless, achieving optimal dispersion in a polymer matrix remains a significant challenge for creating efficient composites, mainly because CNTs tend to aggregate [16-17]. The inert nature of CNTs and the lack of functional sites on the surfaces make this dilemma even worse [18]. Conversely, graphene oxide (GO), a major product of graphene, has attracted significant interest for its future applications in the biological field. The large surface area of GO, as well as its hydrophilic properties, is due to the presence of carboxyl and hydroxyl functional groups. In addition, GO through its non-covalent interactions appears to enhance the dispersion of carbon nanotubes [19, 20]. Therefore, multi-wall carbon nanotubes (MWCNTs) in conjunction with graphene oxide could have a beneficial effect that is not achievable when MWCNTs are used alone.
The synergistic combination of GO and MWCNTs offers a promising approach to improve composite performance while minimizing agglomeration and preserving film flexibility. The utilization of GO as a structural bridging and dispersion-mediating agent can potentially enhance nanotube distribution and interfacial interactions within the chitosan matrix, thereby improving mechanical reinforcement, electrical conductivity, thermal stability, and antioxidant functionality simultaneously.

In the present study, we have synthesized synergized nanocomposite films (SNCFs) of chitosan by incorporating graphene oxide and varying weight ratios of multiwalled carbon nanotubes (MWCNTs) via the solution-blending technique. An extensive range of characterization methods was employed to elucidate the synergistic interactions between graphene oxide and varying ratios of MWCNTs, as well as the effect of these interactions on the properties of chitosan.

## 2.0. Materials and Methods

### 2.1 Chemicals and reagents

The following chemicals and materials were acquired from Sigma-Aldrich USA for the purpose of this research: Sulfuric acid ($H_2SO_4$, 99.9% purity), Sodium nitrate ($NaNO_3$, >99.5% purity), Hydrochloric acid (HCl), Potassium permanganate ($KMnO_4$, 99.9% purity), Graphite (fine powder), Chitosan (C3646, 75% deacetylated), Acetic acid ($CH_3COOH$, 99% purity), N, N-Dimethylformamide (DMF), Multiwalled carbon nanotubes (MWCNTs). Furthermore, distilled water was employed where required throughout the course of experimentation.

### 2.2. Preparation of graphene oxide (GO)

A two-step process was used to prepare graphene oxide. Firstly, the graphite oxide was prepared according to the Hummers method [21]. 2.50 g of graphite and 5 g of $NaNO_3$ were put into concentrated $H_2SO_4$ under constant stirring. The suspension was held at 20 °C, and 7.5g of $KMnO_4$ was added, and stirring was carried out. The mixture was stirred and heated at 35 °C for 30 minutes, after which deionized water was added, and the temperature was adjusted to 98 °C for 15 minutes. After the mixture cooled, a 5.0 % $H_2O_2$ solution was added. The graphite oxide was recovered through filtration, washing, and drying of the supernatant. The graphite oxide was subsequently dispersed in N,N-dimethylformamide (DMF) via continuous stirring and sonication to give graphene oxide [22].

### 2.3. Synthesis of synergic nanocomposite films (SNCFs)

Solution blending was used to synthesize both nanocomposite films (NCFs) and synergized nanocomposite films (SNCFs) [23]. To optimize GO concentration, nanocomposite films (NCFs) comprising chitosan (Ch) and GO were synthesized at varying GO concentrations. The methodology involved the systematic combination of a chitosan solution in acetic acid with a GO dispersion in dimethylformamide (DMF). The resulting mixture was stirred continuously and sonicated to achieve homogeneity. After homogenization, the dispersions were cast onto standard glass Petri dishes (~9 cm in diameter) and dried at ambient temperature for 12 hours, followed by an additional 12 hours at 60°C to form uniform, free-standing nanocomposite films. Subsequently, the material underwent drying. This procedure was replicated with varying GO concentrations, and it was observed that the NCFs containing 0.05 wt.% GO exhibited superior dispersion and flexibility. Thereafter, this optimized 0.05 wt.% GO dispersion was employed in the synthesis of SNCFs, specifically Ch/0.05 wt.% GO in conjunction with different weight ratios of multiwalled carbon nanotubes (MWCNTs). The synthesis process entailed the integration of the chitosan solution in acetic acid with the 0.05 wt. % GO dispersion in DMF, followed by the incorporation of MWCNT dispersions in DMF. The resultant mixture was stirred thoroughly and sonicated. The final formulation was then dried in a petri dish at ambient temperature for 12 hours, followed by an additional 12-hour drying phase at 60°C to yield the SNCFs (Ch/0.05 wt.% GO/MWCNTs). This protocol was executed with various weight ratios of MWCNTs to investigate their effects on the resulting properties of the SNCFs.

### 2.4. Characterization of the SNCF

Fourier Transform Infrared (FTIR) spectra were collected on a Nicolet 6700 spectrometer (Thermo Electron Corporation) at ambient temperature. The spectral resolution was 4 $cm^{-1}$, and the measurements were taken in the 4000-400 $cm^{-1}$ frequency range. The Smart Lab diffractometer (Rigaku) was used to measure X-ray diffraction (XRD) over the 2θ range from 5° to 90°. TA HDi texture analyzer (Stable Micro Systems) with a 5 kg load cell was used to measure the mechanical properties of the SNCFs. As per ASTM D882-83, tests were performed in triplicate using 90mm × 10 $mm^2$ specimens [24]. JSM-5910 (JEOL Japan) scanning electron microscopy (SEM) was used to characterize surface morphology. Mettler Toledo TGA/SDTA851e was used to test the thermal stability under flowing nitrogen. Samples (6-8 mg) were heated from ambient to 700°C at 20°C/min. A four-point probe configuration measured the electrical conductivity of SNCFs. For this purpose, SNCFs having a dimension of 0.5×3.5 $cm^2$ were used [25].

### 2.5. Antioxidant Activity

1.0 $cm^2$ SNCF sample was incubated with 2, 2′-azinobis- (3-ethylbenzothiazoline-6-sulfonic acid) (ABTS). The solution's absorbance was measured in the presence and absence of the SNCFs, allowing calculation of antioxidant activity using equation [26].

$$Inhibition\ (\%) = \frac{Absorbance\ of\ control - Absorbance\ of\ bionanocomposite\ films}{Absorbance\ of\ control} \times 100$$

## 3.0. Results and Discussion

### 3.1. FTIR Spectral analysis

The Fourier Transform Infrared (FTIR) spectra of pristine chitosan (Ch), graphene oxide (GO), Ch/0.05 wt.% GO NCFs, Ch/0.05 wt.% multiwalled carbon nanotubes (MWCNTs) NCFs, and synergized nanocomposite films (SNCFs) containing 0.05 wt.% GO with varying MWCNTs concentrations is presented in Figure (1). The Fourier Transform Infrared (FTIR) spectra of chitosan (Ch), graphene oxide (GO), and chitosan/0.05 wt.% GO nanocomposite films (NCF),

chitosan/0.05 wt.% multiwalled carbon nanotubes (MWCNTs) NCF, and chitosan/0.05 wt.% GO/MWCNTs SNCFs having different weight ratios of MWCNTs as shown in Figure (1). The FTIR spectrum of chitosan exhibits a strong peak at 3400 $cm^{-1}$, which is ascribed to vibrations of O-H and N-H functional groups. In addition, it shows peaks at 1650 $cm^{-1}$ and 1590 $cm^{-1}$, corresponding to the amide I stretching vibration and the amide II N-H bending vibration of the $NH_2$ group, respectively. The spectral peaks in the range of 2800-3000 $cm^{-1}$ are linked to the C-H stretching vibrations, whereas those that occur in the range of 900-1150 $cm^{-1}$ are related to the alcohol and primary amine functionalities that exist in the chitosan structure [27]. In the case of Graphene oxide, the FTIR spectrum shows three clear peaks at 1070 $cm^{-1}$, 1380 $cm^{-1}$, and 1730 $cm^{-1}$, corresponding to C-O-C, C-OH, and COOH, respectively. Moreover, a significant band at 3300 $cm^{-1}$ indicates the occurrence of OH groups. In the FTIR spectrum of Ch/0.05 wt.% GO NCF the characteristic peaks of both components (Ch and GO) remain evident. However, the amide I, amide II, and hydroxyl bands exhibit noticeable broadening and slight shifts toward lower frequencies. These spectral changes indicate the formation of strong hydrogen-bonding interactions between chitosan and GO, suggesting enhanced interfacial compatibility [28]. Likewise, the Ch/0.05 wt.% MWCNTs NCF spectrum shows peaks in the 750-840 $cm^{-1}$ and 840-900 $cm^{-1}$ regions, which can be attributed to the meta-distribution process associated with the benzene rings of MWCNTs [29]. FTIR spectra of SNCFs with different MWCNT ratios show peaks characteristic of chitosan, GO, and MWCNTs. Increasing MWCNT loading results in progressive broadening of the amide and hydroxyl bands, suggesting stronger secondary intermolecular interactions. Furthermore, the gradual reduction in intensity of the GO's C–O stretching peak at 1070 $cm^{-1}$ with increasing MWCNT concentration indicates possible π–π stacking interactions between GO sheets and nanotube surfaces. Mutually, these spectral modifications confirm the successful incorporation of both nanofillers and demonstrate the formation of a hydrogen-bonded, π–π-stacked hybrid network. Such enhanced interfacial interactions are expected to facilitate efficient stress transfer, improve electron transport pathways, and contribute to multifunctional performance enhancement in SNCFs

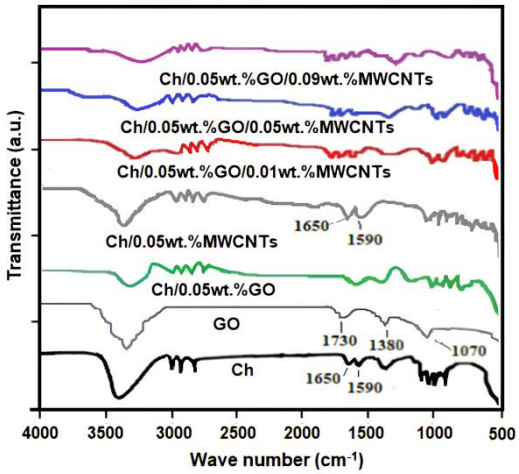


**Figure (1): FTIR spectrum of Ch, GO, Ch/0.05 wt. %GO NCF, Ch/0.05 wt. % MWCNTs NCF and Ch/0.05 wt. % GO / MWCNTs SNCFs with varying contents of MWCNTs**

### 3.2. XRD Analysis

Figure (2) outlines the X-ray diffractograms of chitosan (Ch), graphene oxide (GO), multiwalled carbon nanotubes (MWCNTs) and the chitosan-based NCF containing 0.05 wt.% GO (Ch/0.05 wt.% GO NCF), the chitosan-based NCF consisting of 0.05 wt.% MWCNTs (Ch/0.05 wt.% MWCNTs NCF) and the SNCFs made out of chitosan and 0.05 wt.% GO combined with varying weight contents of MWCNTs. X-ray diffraction (XRD) pattern of pristine chitosan shows a broad diffraction peak at 2θ = 20.9°, which is typical of its semicrystalline characteristics, an attribute arising from ordered regions formed by hydrogen bonding between the polymer chains. Also, the shoulder at 2Θ = 15.1° corresponds to amorphous domains. The GO shows an evident peak at 2Θ = 9.1°, corresponding to the (001) plane, with an increase in interlayer spacing to about 0.97nm, owing to the presence of oxygen-containing functional groups and water molecules between the structural layers. Comparatively, the MWCNTs exhibit diffraction peaks of 2Θ=26.1° and 43°, respectively, which corresponds to planes (002) and (100) of the graphitic carbon, indicating that MWCNTs are highly crystalline and graphitic in nature [30, 31]. A clear peak is observed at 25° in the diffractogram of the Ch/0.05 wt.% GO NCF, and the characteristic peak of GO at 9.1° does not appear. The absence of this peak indicates exfoliation and a homogeneous distribution of GO sheets throughout the chitosan structure, suggesting strong interfacial interactions between chitosan and GO, such as hydrogen bonding and electrostatic repulsion. On the other hand, the diffraction pattern of Ch/0.05 wt.% MWCNTs NCF shows a broad peak of chitosan at around 20.9°, with slight shifts and broadening. This finding suggests that crystallinity is partially reduced and the ordered structure of chitosan is disturbed, likely due to the intercalation or physical entanglement of MWCNTs with the polymer chains. Furthermore, the diffractogram of SNCFs shows that as the MWCNT loading increases from 0.01 wt.% to 0.09 wt.% there is a progressive intensification and sharpening of the peak

at about 26.1°, which corresponds to the (002) plane of MWCNTs, confirming enhanced graphitic network formation and structural integration within the polymer matrix. Importantly, the absence of separate crystalline filler peaks indicates effective nanofiller dispersion without phase separation. These structural modifications support the development of interconnected hybrid filler networks that are critical for improving mechanical strength and electrical conductivity.

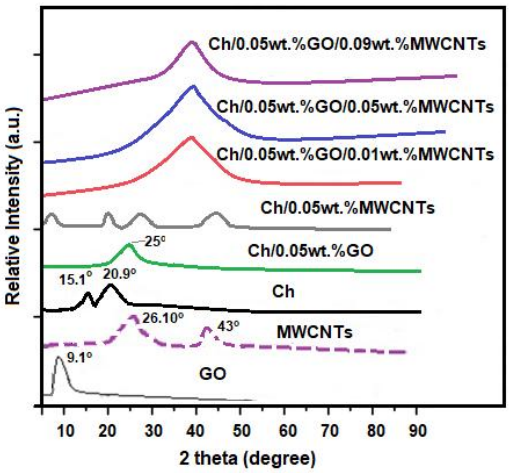


**Figure (2): X-ray diffractogram of Ch, GO, MWCNTs, Cs/0.05 wt. % GO NCF, Ch/0.05 wt.% MWCNTs NCF and Ch/0.05 wt.% GO/MWCNTs SNCFs with varying content of MWCNTs**

## 3.3. Thermal gravimetric analysis

A comprehensive investigation was carried out to evaluate the thermal stability of chitosan (Ch), Ch/0.05 wt. % GO NCF, Ch/0.05wt.% MWCNTs NCF and Ch/0.05wt.GO/MWCNTs SNCFs with different MWCNTs contents, in nitrogen ambient in the temperature span of 25 to 700°C, and the results were plotted in Figure (3). In case of Chitosan (a) it is observed that moisture content starts to decrease at around 100°C whereas the degradation of chitosan moieties takes place between 174-270°C [32]. This process of degradation can presumably be explained by depolymerization and subsequent elimination of glycosidic units [33]. It was observed that at 700°C, approximately 43% of the residue remained. In the Ch/0.05 wt. % GO NCF (b): a 5% weight loss is observed at a temperature range of 180 to 250°C, after which there is a further reduction in weight in the temperature range of 260 to 320 °C. In comparison, the weight remaining at 700°C is about 55%, indicating improved thermal stability compared to the pure chitosan film. In the case of Ch/0.05 wt. % MWCNTs NCF (c), weight loss is first observed at the temperature between 200 and 260°C, and a further degradation is found at between 260 and 350 °C. The weight remaining at 700 oC is 59%, indicating higher thermal stability than the Ch/0.05 wt. % GO. The combination of GO and varying weight contents of MWCNTs with chitosan produced SNCFs (Ch-0.05wt%GO/MWCNTs), and the thermal stability in this case depends directly on the weight ratio of MWCNTs. At 700°C, the increase in the weight ratio of MWCNTs from 0.01 to 0.09 wt. % (as shown in d-f), the residual weight % age rises from 63% to 70%. This enhancement is attributed to the synergistic barrier effect of GO and MWCNTs, which restricts polymer chain mobility, inhibits thermal diffusion, and promotes char formation. The hybrid nanofiller network likely acts as a heat-resistant scaffold, delaying thermal decomposition and enhancing overall structural integrity.

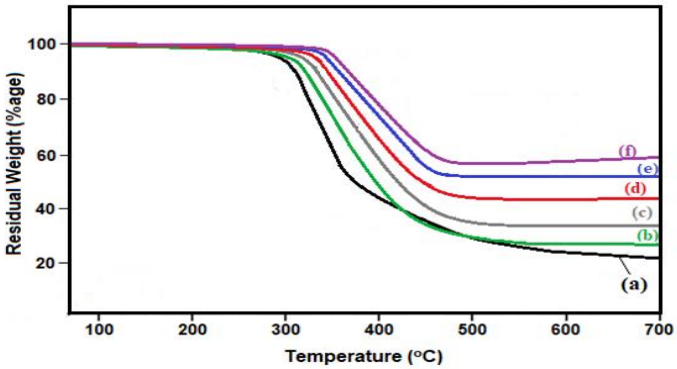


**Figure (3): Thermal gravimetric analysis of (a) Ch (b) Ch/0.05wt.%GO NCF c) Ch/0.05wt. %MWCNTs NCF d) Ch/0.05wt. % GO / 0.01 wt. % MWCNTs, (e) Ch/0.05 wt. % GO/0.05wt. % MWCNTs and (f) Ch/0.009 wt. % GO/ 0.009wt. %MWCNTs SNCFs**

## 3.4. SEM Analysis

Scanning electron microscopy (SEM) was used to investigate the surface morphology of pure chitosan, its nanocomposites, and synergized nanocomposite films (Fig. 4). It was observed in Figure 4(a) that the surface morphology of chitosan (Ch), which appears smooth and featureless, implies a homogeneous polymer. This morphology is typical of

pure chitosan and corresponds to its inherent limitations in mechanical strength and thermal stability. Figure 4(b) shows the Ch/0.05 wt.% GO NCF, and embedded sheets of GO can be seen in the matrix. The sheet-like structures observed are rough, indicating that GO was successfully incorporated and dispersed in the chitosan matrix. The wrinkled appearance can be explained by interfacial stress between chitosan and the rigid GO nanosheets, which enhances mechanical interlocking and, consequently, increases the composite's mechanical properties. Figure 4(c) outlines the Ch/0.05 wt.% MWCNTs NCF, which is a web-like, entangled network of nanotubes. Lastly, Figure 4(d) depicts the Ch/0.05 wt.% GO/0.09 wt.% MWCNTs SNCF, which exhibits a highly porous, networked structure. This morphology indicates synergistic dispersion of GO and MWCNTs and suggests improved interfacial bonding within the polymer matrix. The formation of continuous hybrid filler networks is particularly important for simultaneously enhancing mechanical reinforcement and electrical conductivity.

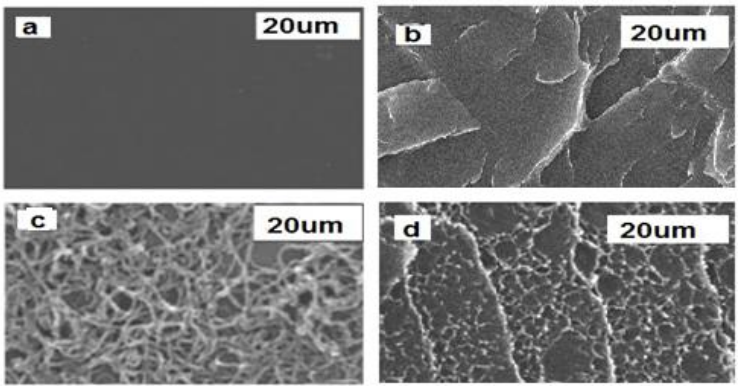


**Figure (4): SEM images of a) Ch (b) Cs/0.05 wt.% GO NCF (c) Ch/0.05 wt.%MWCNTs NCF (d) Ch/0.05 wt.% GO/0.09 wt.% MWCNTs SNCF**

### 3.5. Mechanical analysis

The mechanical behavior of SNCFs reinforced with chitosan and graphene oxide (GO) and varying concentrations of multiwalled carbon nanotubes (MWCNTs; 0.01–0.09 wt.%) was systematically evaluated. Key mechanical parameters, including tensile strength, Young's modulus, and elongation at break, are presented in Figures 5a, 5b, and 5c, respectively. All reported values represent the mean of three independent tensile measurements (n = 3) conducted in accordance with ASTM D882-83 [24]. Error bars represent the standard deviation (±SD), reflecting experimental variability and measurement reproducibility.

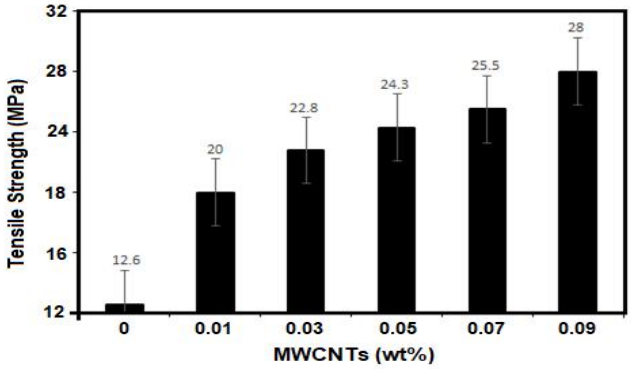


**Figure (5a): Effect of various contents of MWCNTs on tensile strength of Ch/0.05 wt. % GO/MWCNTs SNCF**

Figure (5a) illustrates the effect of MWCNT concentration on the tensile strength of the SNCFs. Tensile strength, defined as the maximum stress a material can withstand before fracture, shows a pronounced dependence on MWCNT loading. The tensile strength of the chitosan/GO film without MWCNTs is approximately 12 MPa, which progressively increases to about 28 MPa at 0.09 wt.% MWCNTs. This substantial enhancement is attributed to the formation of a synergistic reinforcing network within the polymer matrix [34]. MWCNTs function as high-aspect-ratio, load-bearing fillers, while graphene oxide facilitates their uniform dispersion and enhances interfacial compatibility with chitosan [35]. Strong hydrogen bonding interactions between chitosan and GO, together with π–π stacking interactions between GO and MWCNTs, promote efficient stress transfer from the polymer matrix to the rigid carbon nanofillers, thereby suppressing crack propagation [36, 37]. As the MWCNT content increases, a more interconnected reinforcing network is formed, enabling more effective stress distribution and delaying crack initiation and propagation. Consequently, slippage at the filler–matrix interface is minimized, resulting in improved load transfer efficiency and a continuous increase in tensile strength. In Figure 4a, the relatively small error bars across all compositions indicate good uniformity in film preparation and consistent filler dispersion. Although slightly larger deviations are observed at higher MWCNT loadings, likely due to minor local heterogeneities, these variations remain within acceptable limits. Importantly, the progressive separation of the mean tensile strength values with increasing MWCNT content exceeds the corresponding standard deviations,

confirming that the observed enhancement is statistically significant and directly attributable to the reinforcing effect of MWCNTs.

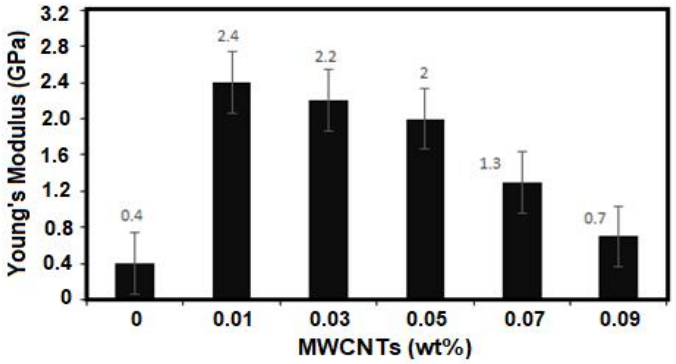


**Figure (5b): Effect of various contents of MWCNTs on Young's modulus of Ch/0.05 wt. % GO/MWCNTs SNCF**

The variation in Young's modulus with MWCNT content is shown in Figure (5b). Young's modulus, which reflects material stiffness, also exhibits a strong dependence on nanofiller concentration. Pure chitosan exhibits a relatively low modulus, consistent with its flexible, ductile polymeric nature. The incorporation of a small amount of MWCNTs results in a sharp increase in stiffness, with the modulus reaching a maximum value of approximately 2.4 GPa at 0.01 wt.% MWCNT loading. This pronounced initial enhancement indicates that even a very low concentration of well-dispersed MWCNTs is sufficient to significantly restrict polymer chain mobility. However, further increases in MWCNT content beyond 0.01 wt.% lead to a gradual decrease in Young's modulus. This reduction may be associated with partial agglomeration of MWCNTs at higher loadings, which can disrupt uniform stress transfer and act as stress concentration sites [38]. In addition, excessive filler content may reduce the reinforcing efficiency per unit filler by interfering with optimal filler matrix interactions [39]. Despite this decline, the modulus values of all SNCFs remain higher than those of pure chitosan, confirming the overall stiffening effect of carbon nanofiller incorporation. In Figure (5b), the low standard deviation is observed at low MWCNTs concentrations, particularly at 0.01 wt.%, suggesting excellent dispersion and uniform mechanical behavior. Slightly increased variability at higher loadings reflects minor heterogeneities but remains indicative of good experimental control. The distinct increase in modulus at low MWCNT content, followed by a gradual decrease at higher loadings, represents a reproducible and statistically meaningful trend rather than random experimental variation.

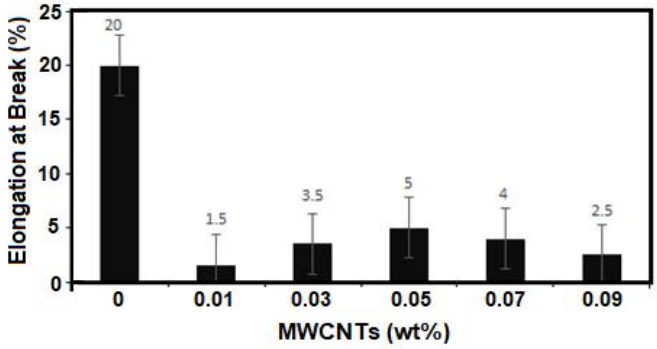


**Figure (5c): Effect of various contents of MWCNTs on elongation at break of Ch/0.05 wt.% GO/MWCNTs SNCF**

Figure (5c) presents the elongation at break of the SNCFs as a function of MWCNT content. Elongation at break, a measure of ductility and flexibility, decreases sharply with the incorporation of MWCNTs. Pure chitosan exhibits the highest elongation at break (approximately 19.5%), reflecting its flexible polymer backbone and ability to undergo significant deformation before fracture. The introduction of only 0.01 wt.% MWCNTs results in a drastic reduction in elongation at break to below 2%, indicating a transition from ductile to brittle behavior [40]. With further increases in MWCNT loading (0.03–0.09 wt.%), the elongation at break remains low. However, minor fluctuations or slight recoveries may occur at intermediate concentrations. These modest variations may be related to improved filler dispersion or partial nanofiller reorientation that locally accommodates deformation.

Nevertheless, the overall ductility of the SNCFs remains significantly lower than that of pure chitosan, highlighting the inherent trade-off between mechanical reinforcement and flexibility in nanofiller-reinforced polymer systems [41]. The pronounced reduction in elongation at break is primarily due to reduced polymer chain mobility resulting from the incorporation of rigid nanofillers. The high stiffness and aspect ratio of MWCNTs promote the formation of a rigid, percolated reinforcing network that limits chain sliding, rotation, and reorganization under tensile stress [42]. Furthermore, strong interfacial interactions-such as hydrogen bonding between chitosan and graphene oxide and π–π stacking between GO and MWCNTs enhance stress transfer but simultaneously anchor polymer chains to the filler

surfaces, reducing energy dissipation mechanisms associated with plastic deformation. At higher MWCNT loadings, localized agglomeration may further contribute to embrittlement by acting as stress concentration sites that facilitate early crack initiation and rapid propagation [43]. In Figure 5c, pure chitosan exhibits relatively larger standard deviations due to its higher ductility and sensitivity to minor variations in film thickness and microstructure.

In contrast, MWCNT-containing SNCFs display smaller standard deviations, indicating more uniform and reproducible fracture behavior. This consistency supports the conclusion that the observed reduction in elongation at break is an intrinsic material response to nanofiller incorporation rather than an artifact of experimental variability. The observed trends in mechanical properties reveal a fundamental trade-off between mechanical strength and flexibility. Tensile strength increases with increasing MWCNT content, whereas stiffness reaches a maximum at low MWCNT loading, accompanied by a pronounced reduction in flexibility at all nanofiller concentrations. These results underscore the critical importance of controlled nanofiller dispersion and optimized filler loading as key parameters for tailoring the mechanical performance of the nanocomposite films to meet specific application requirements. Although the reduction in elongation at break is a common limitation in nanofiller-reinforced polymer systems, several strategies—such as the incorporation of plasticizers and the surface functionalization of MWCNTs may be employed to restore or enhance flexibility without compromising mechanical strength [44].

### 3.6. Electrical conductive analysis

Neat chitosan exhibits essentially insulating behavior, with electrical conductivity approaching 0 $S.cm^{-1}$, consistent with its intrinsically nonconductive polymeric nature. The incorporation of graphene oxide alone, as in the chitosan/0.05 wt.% GO nanocomposite film does not result in a significant change in electrical conductivity. This limited effect is attributed to the presence of abundant oxygen-containing functional groups on GO, which disrupt the $sp^2$-conjugated carbon network and hinder efficient electron transport [45]. In contrast, the addition of multiwalled carbon nanotubes (MWCNTs), as in the chitosan/0.05 wt.% MWCNT nanocomposite film produces a modest increase in conductivity. However, the enhancement remains limited due to the very low MWCNT loading, which is insufficient to establish a fully percolated conductive network within the polymer matrix [46]. A pronounced increase in electrical conductivity is observed when GO and MWCNTs are simultaneously incorporated into the chitosan matrix, as shown for the chitosan/0.05 wt.% GO/MWCNT SNCFs with varying MWCNT contents (Figure 6). The electrical conductivity gradually increases with increasing MWCNT loading, reaching a maximum value of approximately $1.0 \times 10^{-3}$ $S.cm^{-1}$ at 0.09 wt.% MWCNTs. The conductivity values reported in Figure 5 represent the mean of three independent measurements (n = 3) obtained using a four-point probe technique, with error bars denoting the standard deviation (± SD). The observed enhancement in electrical conductivity is attributed to the formation of a percolated conductive network composed of interconnected GO sheets and MWCNTs, which facilitates electron transport through the nanocomposite [47]. The synergistic interaction between GO and MWCNTs, particularly through π–π stacking interactions, promotes effective interfacial contact and network formation even at relatively low filler concentrations [48]. A sharp increase in conductivity is observed in the MWCNT loading range of 0.03–0.05 wt.%, indicating that the electrical percolation threshold lies within this concentration window [49]. Beyond the percolation threshold, MWCNTs form continuous conductive pathways, significantly enhancing charge-carrier mobility. In this hybrid system, GO acts as an effective bridging agent between adjacent MWCNTs, improving network connectivity and reducing contact resistance [50]. The relatively small standard deviations observed across most compositions indicate stable and reproducible conductivity measurements, reflecting uniform filler dispersion and consistent film thickness. Slightly increased variability near the percolation threshold can be attributed to the high sensitivity of electrical conductivity to minor variations in filler distribution and interparticle spacing within this critical concentration range. Nevertheless, the clear separation of mean conductivity values between successive MWCNT loadings exceeds the associated standard deviations, confirming that the observed electrical conductivity enhancement is statistically significant. Collectively, these results demonstrate that the synergistic combination of GO and MWCNTs effectively transforms inherently insulating chitosan into a conductive nanocomposite material.

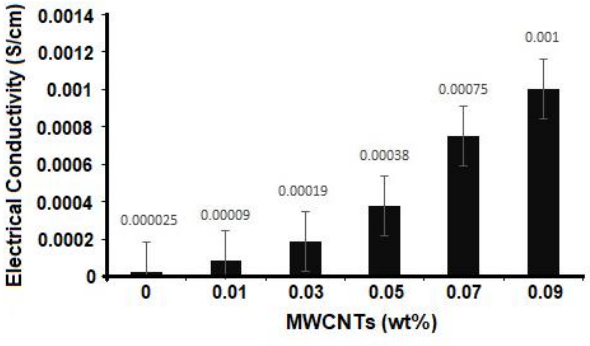


**Figure (6): Effect of various contents of MWCNTs on electrical conductivity of Ch/0.05 wt.% GO/ MWCNTs SNCF**

### 3.7. Antioxidant analysis

Figure (7) shows the effect of increasing MWCNT content on the antioxidant activity of Ch/0.05 wt.% GO/MWCNT synergized nanocomposite films (SNCFs), as evaluated using the ABTS radical scavenging assay. The antioxidant activity values presented in Figure 6 are expressed as mean values obtained from three independent experiments (n = 3) for each film composition. The error bars represent the standard deviation (±SD), indicating the reproducibility and reliability of the ABTS assay. Pure chitosan exhibits relatively low antioxidant activity, which is consistent with its limited ability to donate electrons or hydrogen atoms due to strong intra- and intermolecular hydrogen bonding within the polymer matrix [51]. The incorporation of graphene oxide (0.05 wt.%) into chitosan leads to a modest increase in antioxidant activity. This enhancement is attributed to the presence of oxygen-containing functional groups on GO, which facilitate electron transfer and contribute to partial radical scavenging [52]. Similarly, chitosan films containing MWCNTs alone exhibit a slight improvement in antioxidant performance, owing to the π-conjugated carbon structure of MWCNTs that can interact with and stabilize free radicals [53]. A marked and progressive increase in antioxidant activity is observed when GO and MWCNTs are combined in the SNCFs. As the MWCNT content increases from 0.01 to 0.09 wt.%, the antioxidant activity rises sharply, reaching approximately 90% enhancement at 0.09 wt.% MWCNTs. This significant improvement indicates a strong synergistic effect between GO and MWCNTs in promoting free-radical scavenging efficiency. The pronounced increase in antioxidant activity arises from synergistic electron-transfer mechanisms between GO and MWCNTs embedded in the chitosan matrix. The extended $sp^2$-hybridized carbon networks of MWCNTs allow for efficient delocalization of unpaired electrons generated during radical scavenging, thereby stabilizing reactive species.

Meanwhile, GO provides abundant oxygen-containing functional groups (e.g., hydroxyl, epoxide, and carboxyl groups) that act as active sites for radical interaction. When combined, GO serves as an effective dispersing and bridging agent between adjacent MWCNTs, increasing the accessible surface area and facilitating rapid electron transfer across the hybrid filler network. This cooperative interaction lowers the energy barrier for radical neutralization and suppresses the formation of secondary reactive species. As a result, the SNCFs demonstrate substantially higher antioxidant performance than either single-filler nanocomposites or pure chitosan. The relatively small standard deviations observed across the dataset in Figure (7) reflect good experimental control and uniform interaction between the SNCFs and the ABTS radicals. Slight increases in variability at higher MWCNT loadings may be associated with localized differences in filler distribution or surface exposure; however, these variations remain minimal. Importantly, the separation between mean antioxidant activity values at different MWCNT contents is significantly greater than the corresponding standard deviations, confirming that the observed enhancement is statistically significant rather than due to random experimental error.

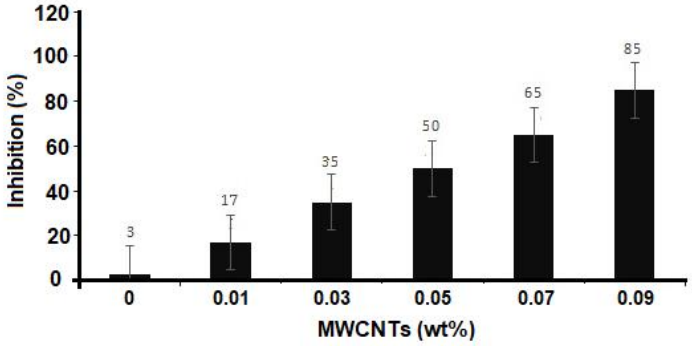


**Figure (7): Effect of various contents of MWCNTs on antioxidant activity of Ch/0.05 wt.% GO/ MWCNTs SNCF**

## 4.0. Conclusion:

The present study demonstrates the successful development of multifunctional synergized nanocomposite films (SNCFs) through the incorporation of graphene oxide and multiwalled carbon nanotubes into a chitosan matrix. Structural and morphological analyses confirmed the formation of a well-dispersed hybrid nanofiller network facilitated by hydrogen bonding and π–π interactions, resulting in significant improvements in mechanical strength, thermal stability, electrical conductivity, and antioxidant activity compared to pristine and single-filler systems. The enhanced multifunctional performance highlights the strong potential of SNCFs for applications in active food packaging, biomedical coatings, and flexible electronic materials, where mechanical durability, electrical responsiveness, and oxidative protection are essential. However, the reduction in elongation at break indicates a strength–flexibility trade-off that may limit applications requiring high mechanical deformability. Additionally, challenges related to large-scale processing, solvent-based fabrication, and potential cytotoxicity of carbon nanofillers require further investigation to ensure industrial scalability and biological safety. Overall, the study establishes an effective hybrid nanofiller strategy for designing high-performance biodegradable nanocomposite films and provides valuable insights for future development of sustainable multifunctional materials.

**Acknowledgment**

The author would like to thank the LEJ Nanotechnology Center, H.E.J. Research Institute of Chemistry, for the use of its laboratory facilities during this research.

**Author's Contribution:** Srosh Fazil (supervised the work), Khurram Liaqat and Danish Anwar (wrote original Manuscript), Imtiaz Hussain (Conducted antioxidant activity), Syed Fakhar Alam (Conducted all other characterizations).

**Conflicts of Interest**

The authors declare no conflicts of interest.

**Funding Source**

**NA**

**References**

1. Kaur, G., Adhikari, R., Cass, P., Bown, M., & Gunatillake, P. (2015). Electrically conductive polymers and composites for biomedical applications. *RSC Advances*, *5*, 37553-37567. https://doi.org/10.1039/C5RA01851J
2. Golafshan, N., Kharaziha, M. & Fathi, M. (2017). Tough and conductive hybrid graphene-PVA: alginate fibrous scaffolds for engineering neural construct. *Carbon*, *111*, 752-763. https://doi.org/10.1016/j.carbon.2016.10.042
3. Kim, H., Lee, H., Seong, K.Y., Lee, E., Yang, S.Y. & Yoon, J. (2015).Visible light-triggered on demand drug release from hybrid hydrogels and its application in transdermal patches. *Advanced Health Care Materials*, *4*, 2071-2077. https://doi.org/10.1002/adhm.201500323
4. Shin, S. R., Shin, C., Memic, A., Shadmehr, S., Miscuglio, M., Jung, H.Y., Jung, S.M., Bae, H., Khademhosseini, A., Tang, X. & Dokmeci, M. R. (2015). Aligned carbon nanotube-based flexible gel substrates for engineering biohybrid tissue actuators. Advanced Functional *Materials*, *25*(28), 4486-4495. https://doi.org/10.1002/adfm.201501379
5. Roodenburg, B., De Haan, S.W.H., Ferreira, J. A., Coronel, P., Wouters, P. C. & Hatt, V. (2013). Toward 6 log 10 pulsed electric field inactivation with conductive plastic packaging material. *Journal of Food Process Engineering*, *36*(1), 77-86. https://doi.org/10.1111/j.1745-4530.2011.00655.x
6. Siripatrawan, U. & Kaewklin, P. (2018). Fabrication and characterization of multifunctional active food packaging from chitosan-titanium dioxide nanocomposite as ethylene scavenging and antimicrobial film. Food Hydrocolloids, 84, 125-134. https://doi.org/10.1016/j.foodhyd.2018.04.049
7. Motiei, M., Kashanian, S., Lucia, L. A. & Khazaei, M. (2017). Intrinsic parameters for the synthesis and tuned properties of amphiphilic chitosan drug delivery nanocarriers. *Journal of Controlled Release*, *260*, 213-225. https://doi.org/10.1016/j.jconrel.2017.06.010
8. Ngo, D.H. & Kim, S.K. (2014). Chapter two- Antioxidant effects of chitin, chitosan, and their derivatives. *Advances in Food and Nutrition Research*, *73*, 15-31. https://doi.org/10.1016/B978-0-12-800268-1.00002-0
9. Qiu, M., Wu, C., Ren, G., Liang, X., Wang, X. & Huang, J. (2014). Effect of chitosan and its derivatives as antifungal and preservative agents on postharvest green asparagus. *Food Chemistry*, *155*, 105-111. https://doi.org/10.1016/j.foodchem.2014.01.026
10. Fernandez-Saiz, P., Lagarón, J. M. & Ocio, M. J. (2009). Optimization of the film-forming and storage conditions of chitosan as an antimicrobial agent. *Journal of Agricultural and Food Chemistry*, *57*(8), 3298-3307. https://doi.org/10.1021/jf8037709
11. Zhou, T., Qi, X., Bai, H. & Fu, Q. (2016). The different effect of reduced graphene oxide and graphene oxide on the performance of chitosan by using homogenous fillers. *RSC Advances*, *6*(41), 34153-34158. https://doi.org/10.1039/C6RA02225A
12. Karimi, A.R. & Khodadadi, A. (2016). Mechanically robust 3D nanostructure chitosan-based hydrogels with autonomic self-healing properties. *ACS Applied Materials and Interfaces*, *8*(40), 27254-27263. https://doi.org/10.1021/acsami.6b10375
13. Spitalsky, Z., Tasis, D., Papagelis, K. & Galiotis, C. (2010). Carbon nanotube-polymer composites: chemistry, processing, mechanical and electrical properties. *Progress in Polymer Science*, *35*(3) 375-401. https://doi.org/10.1016/j.progpolymsci.2009.09.003
14. Sun, Y. & Shi, G. (2013). Graphene/polymer composites for energy applications. *Journal of Polymer Science B. Polymer Physics*, *51*, 231-253. https://doi.org/10.1002/polb.23226
15. Yadav, S. K. & Cho. J. W. (2013). Functionalized graphene nanoplatelets for enhanced mechanical and thermal properties of polyurethane nanocomposites. *Applied Surface Science*, *266*, 360-367. https://doi.org/10.1016/j.apsusc.2012.12.028
16. DE-Volder, M. F. L., Tawfick, S. H., Baughman, R. H. & Hart, A. J. (2013). Carbon nanotubes: present and future commercial applications. *Science*, *339*(6119), 535-539. https://doi.org/10.1126/science.1222453
17. Tang, L.C., Wan, Y. J., Peng, K., Pei, Y. B., Wu, L. B., Chen, L. M., Shu, L. J., Jiang, J. X. & Lai, G. Q. (2013). Fracture toughness and electrical conductivity of epoxy composites filled with carbon nanotubes and spherical

particles. *Composites A: Applied Science and Manufacturing*, *45*, 95-101. https://doi.org/10.1016/j.compositesa.2012.09.012
18. Moniruzzaman, M. & Winey, K. I. (2006). Polymer nanocomposites containing carbon nanotubes. *Macromolecules*, *39*(16), 5194-5205. https://doi.org/10.1021/ma060733p.
19. He, Y., Zhang, N., Gong, Q., Qiu, H., Wang, W., Liu, Y.; Gao, J. (2012). Alginate/graphene oxide fibers with enhanced mechanical strength prepared by wet spinning. *Carbohydrates Polymer*. *88*(3), 1100-1108. https://doi.org/10.1016/j.carbpol.2012.01.071
20. Zhang, C., Ren, L., Wang, X. & Liu, T. (2010). Graphene oxide-assisted dispersion of pristine multiwalled carbon nanotubes in aqueous media. *The Journal of Physical Chemistry C*, *114*(26), 11435-11440. https://doi.org/10.1021/jp103745g
21. Hummers Jr., W.S. and Offeman, R. E. (1958). Preparation of graphitic oxide, *Journal of American. Chemical Society*, *80*(6), 1339. https://doi.org/10.1021/ja01539a017
22. Paredes, J. I., Villar-Rodil, S., Matinez-Alonso, A. & Tascon, J. M. D. (2008). Graphene oxide dispersions in organic solvents, *Langmuir*, *24*(19), 10560-10564. https://doi.org/10.1021/la801744a
23. Alver, E., Metin, A.U. & Çiftçi, H. (2014). Synthesis and characterization of chitosan/polyvinylpyrrolidone/zeolite composite by solution blending method. *Journal of Inorganic and Organometallic Polymer and Materials*. *24*, 1048–1054. https://doi.org/10.1007/s10904-014-0087-z
24. Rakas, M. & Jacobine, A. (1992). Mechanical and dynamic mechanical properties of photocrosslinked norbornene-thiol copolymer films. The Journal of Adhesion, 36, 4, 247-263. https://doi.org/10.1080/00218469208026529
25. Ceja, I., Gonzalez-Iniguez, K. J., Carreon-Alvarez, A., Landazuri, G., Barrera, A., Casillas, J. E., Fernandez-Escamilla, V. V. A., & Aguilar, J. (2020). Characterization and electrical properties of PVA films with self-assembled chitosan-AuNPs/SWCNT-COOH nanostructures. *Materials*, *13*(18), 4138. https://doi.org/10.3390/ma13184138
26. Nunes, C., Maricatoa, E., Cunhaa, A., Nunes, A., Lopes da Silvaa, A. J. & Coimbraa., M. A. (2013). Chitosan–caffeic acid–genipin films presenting enhanced antioxidant activity and stability in acidic media. *Carbohydrate Polymers*, *91*(1,2), 236-243. https://doi.org/10.1016/j.carbpol.2012.08.033
27. Azhar, F. F., Olad, A. & Salehi, R. (2014). Fabrication and characterization of chitosan - gelatin/nanohydroxyapatite - polyaniline composite with potential application in tissue engineering scaffolds. *Designed Monomers and Polymers*, *17*(7), 654-667. https://doi.org/10.1080/15685551.2014.907621
28. Yadav, M. & Ahmad, S. (2015). Montmorillonite/graphene oxide/chitosan composite: synthesis, characterizationand properties. *International Journal of Biological Macromolecules*, *79*, 923-933. https://doi.org/10.1016/j.ijbiomac.2015.05.055
29. Malikov, E. Y., Muradov, M. B., Akperov, O. H., Eyvazova, G. M., Puskás, R., Madarász, D., Nagy, L., Kukovecz, Á. & Kónya, Z. (2014). Synthesis and characterization of polyvinyl alcohol based multiwalled carbon nanotube nanocomposites. Physica E: *Low- Dimensional Systems and Nanostructures, 61*, 129-134. https://doi.org/10.1016/j.physe.2014.03.026
30. Aziz, S.B., Abdullah, O. G., Rasheed, M.A. & Ahmed, H. M. (2017). Effect of high salt concentration (HSC) on structural, morphological and electrical characteristics of chitosan based solid polymer electrolytes. *Polymers*, *9*, 187. https://doi.org/10.3390/polym9060187
31. Yu, J., Lu, K., Sourty, E., Grossiord, N., Koning, C. E. & Loos, J. (2007). Characterization of conductive multi-wall carbon nanotube/ polystyrene composites prepared by latex technology. *Carbon*, *45*(15), 2897-2903. https://doi.org/10.1016/j.carbon.2007.10.005
32. Islam, A., Yasin, T., Bano, I. & Riaz, M. (2012). Controlled release of aspirin from pH sensitive chitosan / poly (vinyl alcohol) hydrogel. *Journal of Applied Polymer Science*, *124*(5), 4184-4192. https://doi.org/10.1002/app.35392
33. Carson, L., Kelly-Brown, C., Stewart, M., Oki, A., Regisford, G., Luo, Z.P. & Bakhmutov, V. I. (2009). Synthesis and characterization of chitosan-carbon nanotube composites. Materials Letters, *63*(6-7), 617-620. https://doi.org/10.1016/j.matlet.2008.11.060
34. Pan, Y., Bao, H., & Li, L. (2011). Noncovalently functionalized multiwalled carbon nanotubes by chitosan-grafted reduced graphene oxide and their synergistic reinforcing effects in chitosan films. *ACS Applied Materials & Interfaces*, *3*, 4819-4830. https://doi.org/10.1021/am2013135
35. Navidfar, A. & Trabzon, L. (2026). Recent advances in the multifunctional properties and applications of carbon nanotube/graphene hybrid polymer nanocomposites. *Polymer Composites*, *47*, 1, 29-51. https://doi.org/10.1002/pc.70159
36. Compton, O. C. & Nguyen, S. T. (2010). *Graphene oxide, highly reduced graphene oxide, and graphene: Versatile building blocks for carbon-based materials. Small*, *6*, 711–723. https://doi.org/10.1002/smll.200901934

37. Stankovich, S., Dikin, D. A., Dommett, G. H. B., Kohlhaas, K. M., Zimney, E. J., Stach, E. A., Piner, R. D., Nguyen, S. T. & Ruoff, R. S. (2026). *Graphene-based composite materials.* ***Nature***, ***442***, 282-286. https://doi.org/10.1038/nature04969
38. Polydoropoulou, P. V., Tserpes, K., Pantelakis, S. & Katsiropoulos, C. (2020). Multiscale modeling of polymers filled with MWCNTs: the effect of dispersion, waviness, interphase and agglomerations. *Aircraft Engineering and Aerospace Technology: An International Journal*, 92, 9, 1429-1440. https://doi.org/10.1108/AEAT-11-2019-0230
39. Tazibt, N., Kaci, M., Dehouche, N., Ragoubi, M. & Atanase, L. (2023). Effect of filler content on the morphology and physical properties of poly (lactic acid)-hydroxyapatite composites. *Materials*.*16*, 2, 809. https://doi.org/10.3390/ma16020809
40. Roumeli, E., Avgeropoulos, A., Pavlidou, E., Vourlias, G., Kyratsi, T., Bikiaris, D. & Chrissafis, K. (2014). Understanding the mechanical and thermal property reinforcement of crosslinked polyethylene by nanodiamonds and carbon nanotubes. *RSC Advances*, *4*, 85, 45522-45534. https://doi.org/10.1039/C4RA05585C
41. Muhammad, T. & Akgul, A. (2025). Optimizing mechanical performance of AgC-reinforced polymer nanocomposites: a quantitative analysis of stiffness–ductility trade-offs. Babylonian *Journal of Mechanical Engineering*, 34-50. https://doi.org/10.58496/BJME/2025/003
42. Nurazzi, N. M., Asyraf, M., Khalina, A., Abdullah, N., Sabaruddin, F. A., Kamarudin, S. H., Ahmad, S., Mahat, A. M., Lee, C. L., Aisyah, H. A., Norrrahim, M., Ilyas, R. A., Harussani, M. M., Ishak, M. & Sapuan, S. M. (2021). Fabrication, functionalization, and application of carbon nanotube-reinforced polymer composite: an overview. *Polymers*. *13*(7), 1047. https://doi.org/10.3390/polym13071047
43. Krishnan, A. & Xu, L. R. (2012). A simple effective flaw model on analyzing the nanofiller agglomeration effect of nanocomposite materials. *Journal of Nanomaterials*. *1*. https://doi.org/10.1155/2012/483093
44. Feng, Y., Peng, C., Li, Y. & Hu, J. (2018). Enhanced dielectric and mechanical properties of ternary composites via plasticizer-induced dense interfaces. *Materials*. *11*(7),1111. https://doi.org/10.3390/ma11071111
45. Milka, I. A., Ahadito, B. R., Desnelli, H. N. & Said, M. (2026). A review of graphene oxide and reduced graphene oxide applications: multifunctional nanomaterials for sustainable environmental and energy devices. *Journal of Carbon Research*, *12* (1), 11. https://doi.org/10.3390/c12010011
46. Bauhofer, W. & Kovacs, J. (2009). A review and analysis of electrical percolation in carbon nanotube polymer composites. *Composites Science and Technology*, https://doi.org/10.15480/882.392
47. Wang, B., Dou, S., Li, W. & Gao, Y. (2019). Multifunctional reduced graphene oxide/ carbon nanotubes/epoxy resin nanocomposites based on carbon nanohybrid preform. *Soft Materials*, *18*(1)89-100. https://doi.org/10.1080/1539445X.2019.1688833
48. Zhang, C., Ren, L., Wang, X. & Liu, T. (2010). Graphene oxide-assisted dispersion of pristine multiwalled carbon nanotubes in aqueous media. *Journal of Physical Chemistry C*. *114*, 26, 11435-11440. https://doi.org/10.1021/jp103745g
49. Jouni, M., Faure-Vincent, J., Djurado, D., Fedorko, P. & Boiteux, G. (2014). Low electrical percolation threshold and charge carrier transport in multiwalled carbon nanotube polymer nanocomposites. *Carbon*. http://dx.doi.org/10.1016/j.carbon.2014.04.031
50. Tripathi, M., Valentini, L., Rong, Y., Bon, S. B., Pantano, M. F., Speranza, G., Guarino, R., Novel, D., Iacob, E., Liu, W., Micheli, V., Dalton, A. & Pugno, N. M. (2020). Free-standing graphene oxide and carbon nanotube hybrid papers with enhanced electrical and mechanical performance and their synergy in polymer laminates. *International Journal of Molecular Sciences*, *21*(22), 8585 https://doi.org/10.3390/ijms21228585
51. Ivanova, D. & Yaneva, Z. (2020). Antioxidant properties and redox-modulating activity of chitosan and its derivatives: Biomaterials with application in cancer therapy. *BioResearch Open Access*, *9*(1). https://doi.org/10.1089/biores.2019.0028
52. Wang, Y., Kong, W., Wang, L., Zhang, J., Li, Y., Liu, X. & Li, Y. (2019). Optimizing oxygen functional groups in graphene quantum dots for improved antioxidant mechanism. *Physical Chemistry Chemical Physics*, *21*(3), 1336-1343. https://doi.org/10.1039/C8CP06768F
53. Guan, Y., Yang, R., Huang, Y., Yu, C., Wei, X. Li. & Xu, D X. (2018). Multiwalled carbon nanotubes acting as antioxidant for fluorosilicone rubber. *Polymer Degradation and Stability*, *156*,161-169. https://doi.org/10.1016/j.polymdegradstab.2018.06.018


**Received: January 15th 2026** **Accepted: February 10th 2026**